Supporting Information

Synergistic Radical Generation and Electron Transfer Mechanisms in Oxygen-Deficient Co_3O_4: Bridging Defect Concentration and Catalytic Efficiency in PMS-Based AOPs

Yanjing Zhang, Guanpu Zeng, Rui Lv, Jing Lan, Zongshan Zhao and Guoliang Li*

School of Environment and Geography, Qingdao University, Qingdao 266071, China

*Corresponding author: Guoliang Li, glli@qdu.edu.cn

Text 1 Materials

All chemicals were used without further purification, including cobalt(II) nitrate hexahydrate ($Co(NO_3)_2·6H_2O$, ≥98.5%) 2-methylimidazole (2-MeIm, 98%), methanol (MeOH, 99.9%), sulfuric acid (H_2SO_4, ≥98%), sodium hydrogen carbonate ($NaHCO_3$, ≥99.5%),sodium chloride (NaCl, ≥99.5%), anhydrous sodium sulfate (Na_2SO_4, ≥99%), sodium nitrate ($NaNO_3$, ≥99%), tert-butyl alcohol (TBA, ≥99.5%), p-benzoquinone (pBQ, ≥99%), tetracycline (TC), Potassium monopersulfate triple salt (PMS,42%-46% $KHSO_5$ basis).

Text 2 Sample Preparation

The cubic ZIF-67, acting as template, was firstly synthesized according to previously reported literature with some modification[1].Typically, cobaltous nitrate hexahydrate (464 mg) and CTAB (8 mg) were dissolved in 18 mL deionized water, which labeled as solution A. 2-methylimidazole (5.68 g) was dissolved in 100 mL deionized water and labeled as solution B. Then solution A was quickly poured into solution B and magnetically stirred at room temperature for 30 min, the obtained purple solid was then centrifuged and washed with deionized water and methanol for several times, and finally dried at 70℃ overnight. The obtained ZIF-67 nano cubes were then submitted to a pyrolysis procedure in a tube furnace under flowing Ar at 550℃ (heating rate: 2℃ min-1) for 2 hours, followed by annealing at 250℃ in air for 2 hours. After cooling to room temperature, the samples composed of small Co_3O_4 nanoparticles, named as S-Co_3O_4, were obtained. Accordingly, samples composed of medium sized nanoparticles and larger particles, named as M-Co_3O_4 and B-Co_3O_4 respectively, were synthesized similarly but annealed at 400℃ and 550℃ in air, respectively.

Text 3 Characterization methods

The morphology of catalysts was imaged by scanning electron microscopy (SEM) (GeminiSEM 360) and transmission electron microscopy (TEM) (JEM-F200). X-ray diffraction (XRD) patterns were recorded using a Bruker-D8 Advance with Cu Kα radiation (50–149 kV, 200 mA) in the 2θ range of 10°–80° at a scanning rate of 5°/min. Fourier transform infrared (FT-IR) spectra were obtained on a Thermo Fisher Scientific Nicolet iS20 spectrometer. Surface analysis was performed by X-ray photoelectron spectroscopy (XPS, Thermo Scientific K-Alpha) with monochromatized Al Kα excitation. Reactive oxygen species detection was carried on an electron paramagnetic resonance (EPR, Bruker A300), where $^1O_2$ was trapped with TEMP (2,2,6,6-tetramethylpiperidine) in ultrapure water.

Text 4 Experimental Procedure

Degradation experiment: All experiments were conducted in 50 ml conical flasks. Typically, 20 mg of catalyst was dispersed in 50 ml TC solution (20 mg mL^{-1}) under magnetic stirring at room temperature. The initial pH of the solution was measured and adjusted with 0.1 mol/L H_2SO_4 or NaOH. To initiate the reaction, after loading 1 mM PMS to initiate reaction, 3 ml aliquots were collected at certain intervals, immediately quenched with 1 ml ethanol, filtered through 0.22 μm membranes, and then analyzed at λ = 356 nm via a UV spectrophotometer. Each experiment included triplicate trials, and the observed rate constant (k_{obs}) was calculated via the pseudo-first-order kinetic model:

$$\ln\left(\frac{C}{C_0}\right) = -k_{obs}t \quad \text{S1}$$

Where k_{obs} is the apparent rate constant, C is the TC concentration at time t, and C_0 is the initial concentration of TC.

Electrochemical analysis tests: A Gamry Reference 3000 workstation with a three-electrode system (glassy carbon working electrode, Pt counter electrode, Ag/AgCl reference electrode) in 0.5 M Na_2SO_4 electrolyte was used to investigate the electron transfer in the catalytic system.

Text 5 Quantifying the steady-state concentration of reactive species

The steady state concentrations of •OH, $•SO_4^-$ and $^1O_2$ ($[•OH]_{ss}$, $[•SO_4^-]_{ss}$, $[^1O_2]_{ss}$, M) in the S-Co_3O_4/PMS processes can be calculated using BA, NB and FFA as probe compounds. The probe compounds are at concentration levels (0.2 mg/L for BA, NB and FFA) that would not affect degradation of TC (Fig. S8a). The second-order reaction rate constants between organic compounds and reactive species ($M^{-1}·s^{-1}$) were shown in Table S5.

$$-\ln\frac{[BA]}{[BA]_0}=(k_{BA,·OH}[•OH]_{ss}+k_{BA,•SO_4^-}[•SO_4^-]_{ss})t=k_{obs,BA}t \quad S2$$

$$-\ln\frac{[NB]}{[NB]_0}=(k_{NB,·OH}[•OH]_{ss}+k_{NB,•SO_4^-}[•SO_4^-]_{ss})t=k_{obs,NB}t \quad S3$$

$$-\ln\frac{[FFA]}{[FFA]_0}=(k_{FFA,·OH}[•OH]_{ss}+k_{FFA,•SO_4^-}[•SO_4^-]_{ss}+k_{FFA,\ ^1O_2}[\ ^1O_2]_{ss})t=k_{obs,FFA}t \quad S4$$

The pseudo-first-order reaction rate constants ($k_{obs,BA}$, $k_{obs,NB}$ and $k_{obs,FFA}$) can be obtained from the plots of $-\ln\frac{[BA]}{[BA]_0}$, $-\ln\frac{[NB]}{[NB]_0}$ and $-\ln\frac{[FFA]}{[FFA]_0}$ versus time, respectively (Fig. S9b). Then, $[•OH]_{ss}$, $[•SO_4^-]_{ss}$, $[^1O_2]_{ss}$ can be obtained by solving Equations S2-4. Then, the contribution of $R_{•OH}$, $R_{•SO_4^-}$ and R_{1O2} could be obtained:

$$R_{•OH}=\frac{k_{TC,·OH}[•OH]_{ss}}{k_{TC}} \quad S5$$

$$R_{•SO_4^-}=\frac{k_{TC,•SO_4^-}[•SO_4^-]_{ss}}{k_{TC}} \quad S6$$

$$R_{1O2}=1-R_{•OH}-R_{•SO_4^-} \quad S7$$

Text 6 The mechanism proceeds in the S-Co_3O_4/PMS system

$$Co^{2+}+HSO_5^-\rightarrow Co^{3+}+\bullet SO_4^-+OH^- \quad \text{S8}$$

$$Co^{3+}+HSO_5^-\rightarrow Co^{2+}+\bullet SO_5^-+H^+ \quad \text{S9}$$

$$\bullet SO_4^-+H_2O\rightarrow HSO_4^-+\bullet OH \quad \text{S10}$$

$$\bullet OH+OH^-\rightarrow \bullet O^-+H_2O \quad \text{S11}$$

$$\bullet OH+\bullet O^-\rightarrow HO_2^- \quad \text{S12}$$

$$\bullet OH+HO_2^-\rightarrow OH^-+\bullet HO_2 \quad \text{S13}$$

$$\bullet HO_2\rightarrow H^++\bullet O_2^- \quad \text{S14}$$

$$\bullet O_2^-+2H^+\rightarrow H_2O_2+{}^1O_2 \quad \text{S15}$$

$$2\bullet SO_5^-+H_2O\rightarrow 2HSO_4^-+3/2\ {}^1O_2 \quad \text{S16}$$

$$\bullet SO_4^-+\bullet OH+{}^1O_2+TC\rightarrow \text{by-products}+CO_2+H_2O \quad \text{S17}$$

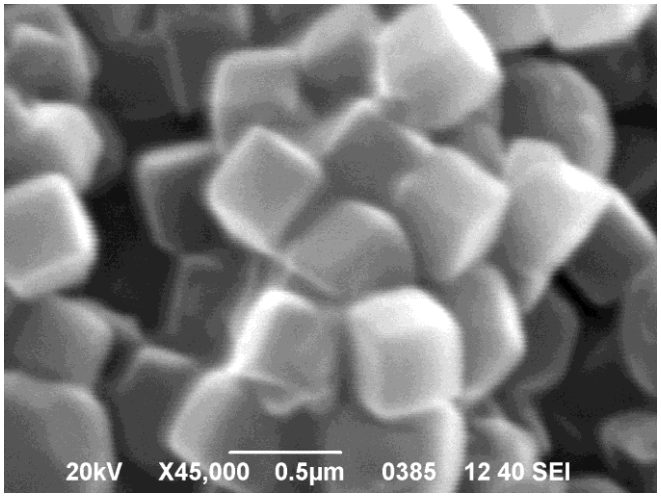

Fig. S1. The SEM images of ZIF-67

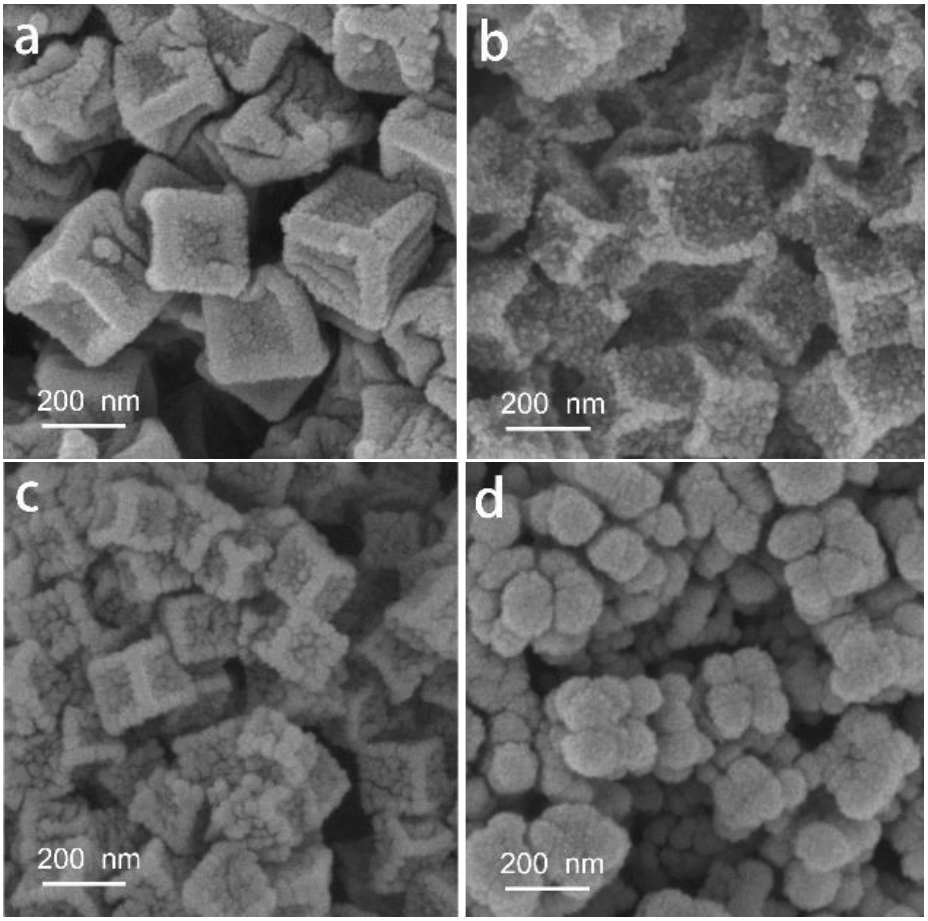

Fig. S2. The SEM images of Co@C (a), S-Co_3O_4 (b), M-Co_3O_4 (c) and B-Co_3O_4 (d).

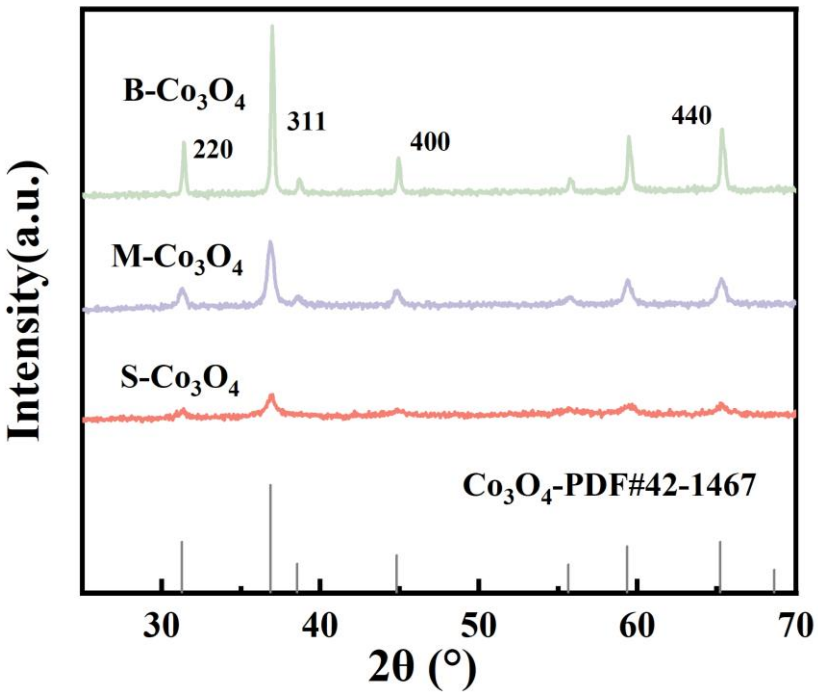

Fig. S3. XRD patterns of S\M\B-Co_3O_4.

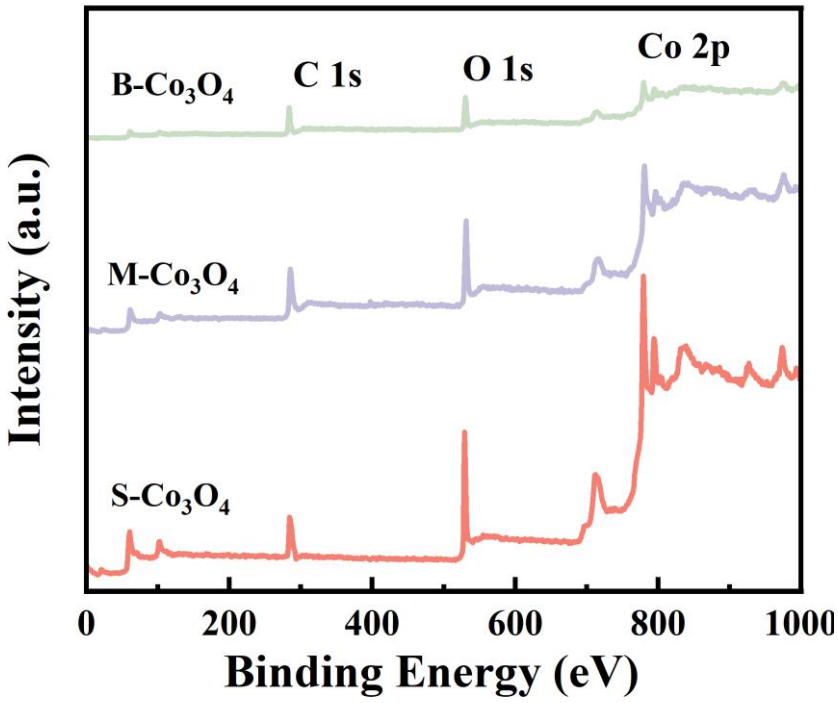

Fig. S4. XPS full spectrum of S/M/B-Co_3O_4.

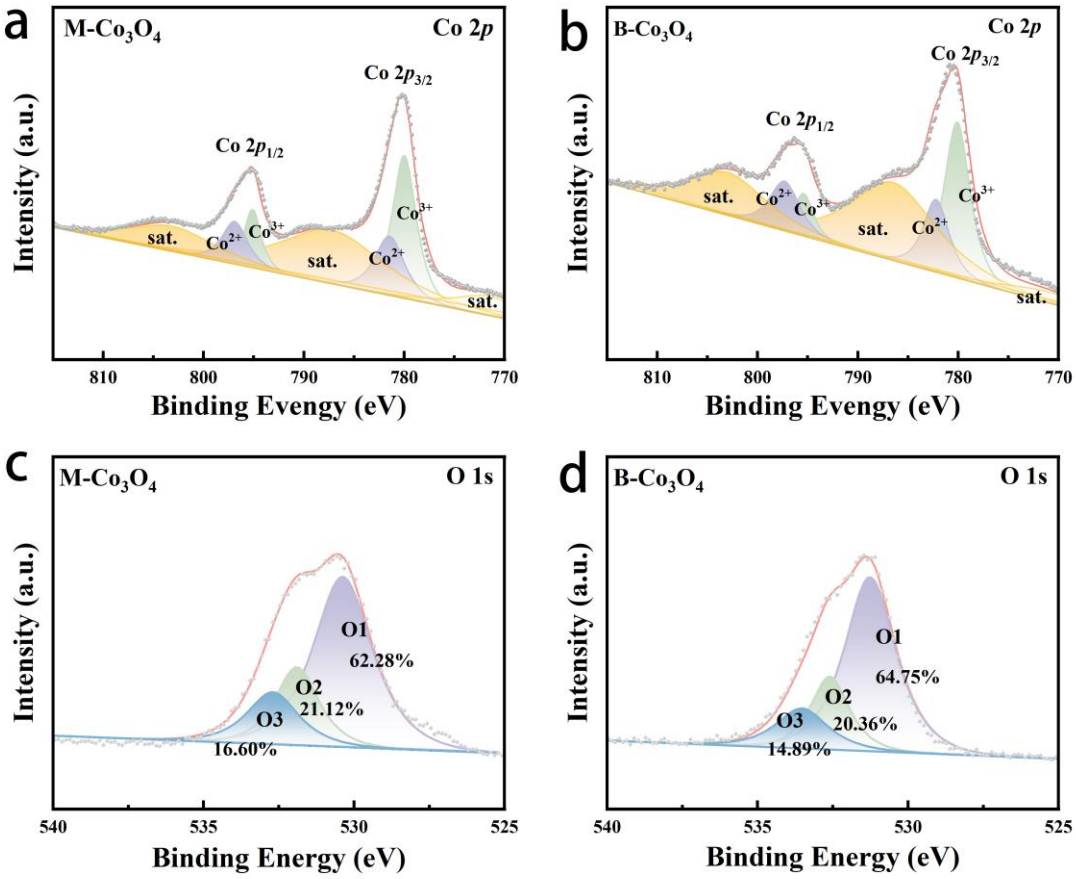

Fig. S5. XPS spectrum of Co 2p (a, b) and O 1s (c, d) of M-Co_3O_4 and B-Co_3O_4, respectively.

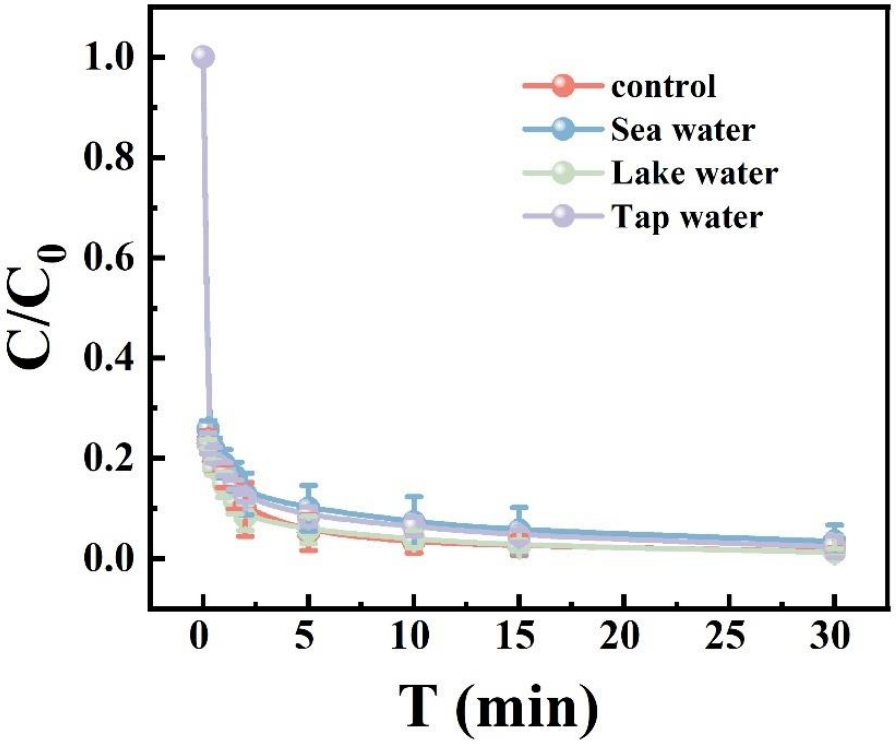

Fig. S6. Different water bodies

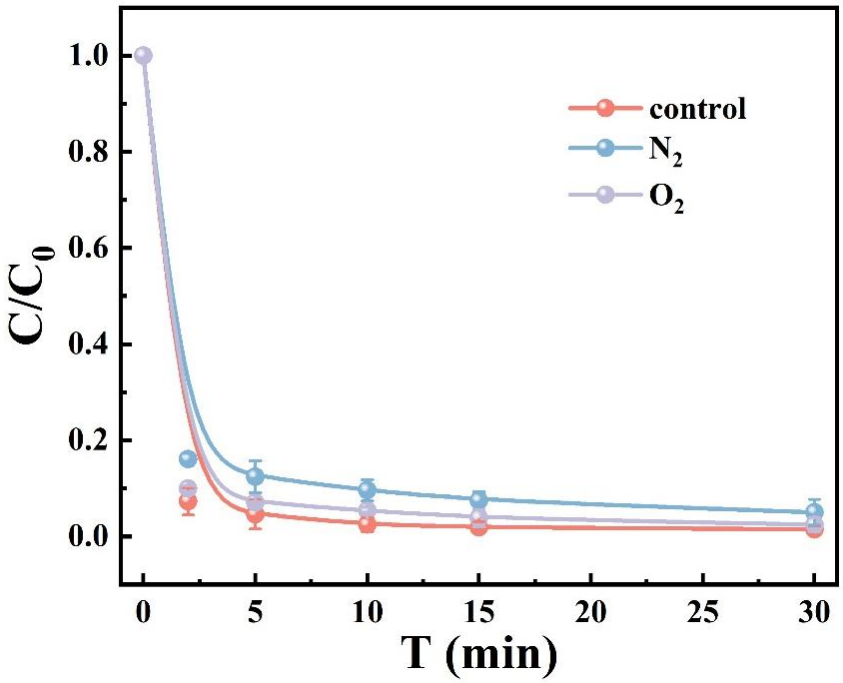

Fig. S7. The influence of different gases on the degradation experiment.

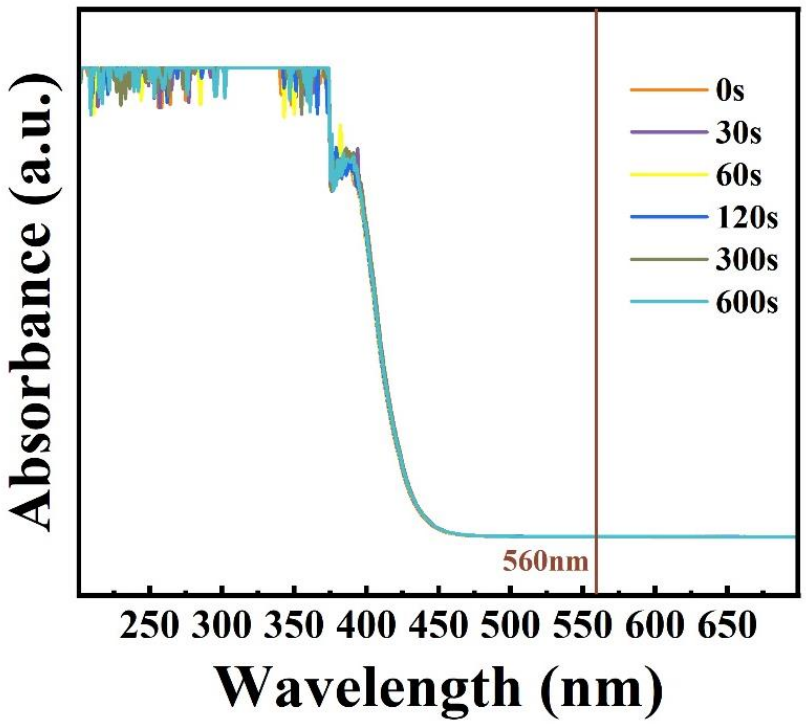

Fig. S8. NBT test of $\bullet O_2^-$.

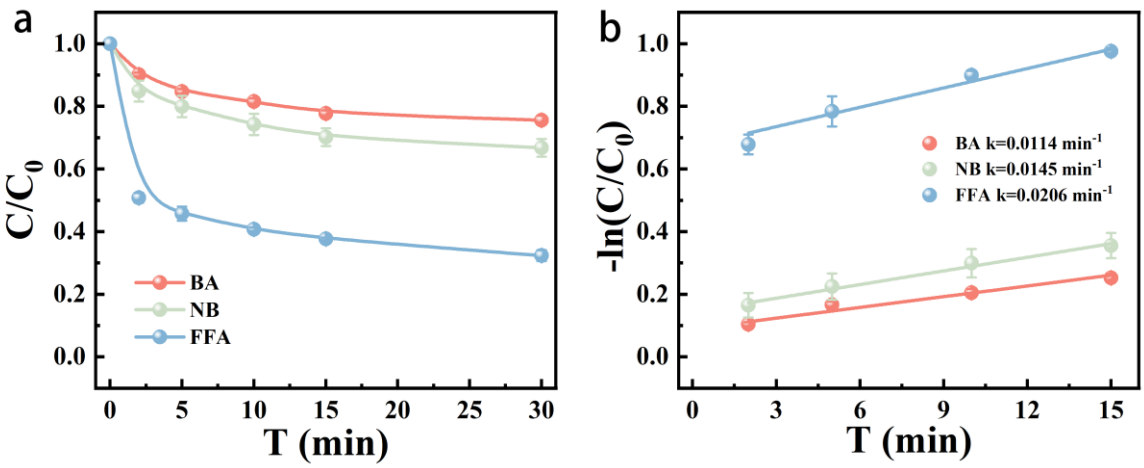

Fig. S9. The degradation(a) and the pseudo first-order kinetic model fitting(b) of probes in S-Co_3O_4/PMS.

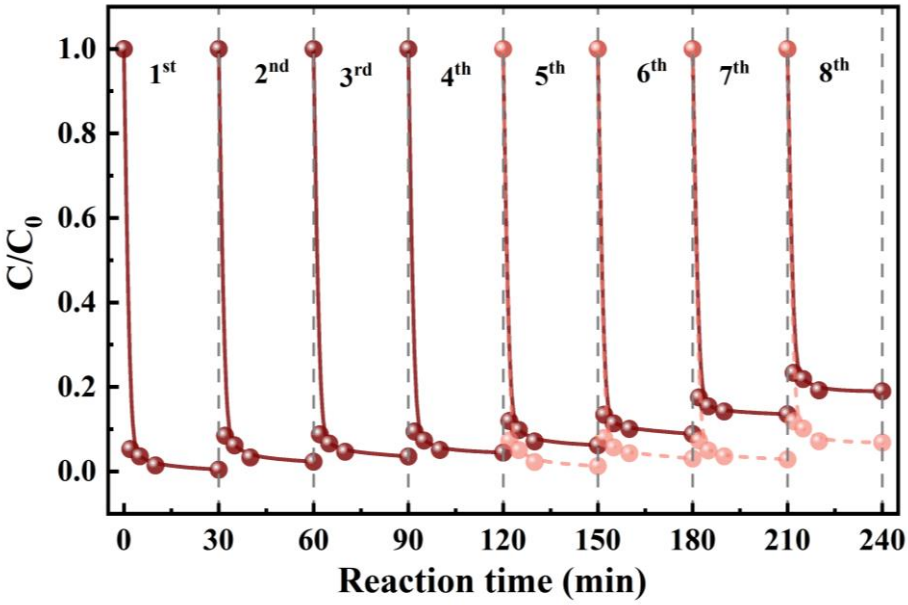

Fig. S10. Catalyst recycling experiment (The deep red solid lines represent the experimental data, and the light red dashed lines represent the calculated compensation data).

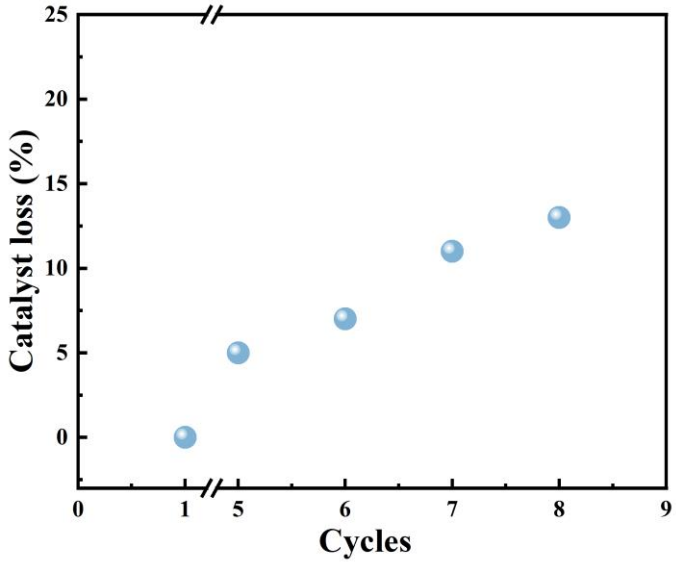

Fig. S11. The dose loss of the catalyst in the cyclic experiment.

Table S1. Comparisons of *S-Co_3O_4* with previously reported metal catalysts for TC degradation by PMS activation.

Catalysts ($g \cdot L^{-1}$)	PMS dosage ($g \cdot L^{-1}$)	Pollutant concentration ($mg \cdot L^{-1}$)	Degradation time(min) and efficiency (%)	Ref.
NiO/SnO_2(0.4)	0.2	20	20/90	2022[2]
Mn-MoS_2@AABs(3.0)	0.4	20	90/80	2022[3]
MIL-101(Fe)/Co_3O_4(0.3)	0.6	100	40/86	2022[4]
Fe-NPC-600(0.2)	0.3	30	20/90	2023[5]
$MnFe_2O_4/MoS_2$ (0.2)	0.3	10	30/92.9	2024[6]
Fe_3O_4@PANI-p (0.4)	4mm	20	90/89.1	2023[7]
Co-CNNT (0.2)	0.8mM	10	24/95.4	2023[8]
S-Co_3O_4(0.4)	**0.3**	**20**	**10/98.6**	**This work**

Table S2. The element content of the as-prepared samples tested by XPS

Sample	Co	O	C
S-Co_3O_4	**10.54**	**30.47**	**58.99**
M-Co_3O_4	12.69	29.68	57.68
B-Co_3O_4	6.10	30.75	63.15

Table S3. XPS of O 1s deconvolution information of different samples.

Sample	*O1*	***O2***	*O3*
S-Co_3O_4	22.96%	**53.88%**	23.16%
M-Co_3O_4	62.28%	**21.12%**	16.60%
B-Co_3O_4	64.75%	**20.36%**	14.89%

Table S4. XPS of Co 2p deconvolution information of different samples.

Sample	Co^{2+}	Co^{3+}	Co^{2+}/Co^{3+}
S-Co_3O_4	**50.48%**	**49.52%**	**101%**
M-Co_3O_4	39.29%	60.71%	64.71%
B-Co_3O_4	40.88%	59.12**%**	69.14%

Table S5. The second-order reaction rate constants between quenchers with various reactive species (M^{-1} s^{-1})[9].

Quencher	Quenched species	$k_{\cdot OH}$	$k_{\cdot SO_4^-}$	$k_{^1O_2}$
Methanol (MeOH)	·OH, $\cdot SO_4^-$	9.7×10^8	1.1×10^7	3.89×10^3
tert-butanol (TBA)	·OH	6×10^8	4×10^5	1.8×10^3
Furfuryl alcohol (FFA)	·OH, $\cdot SO_4^-$, $^1O_2$	1.5×10^{10}	1.3×10^{10}	1.2×10^8

Table S6. The second-order reaction rate constants between probe compounds or TC with various reactive species (M^{-1} s^{-1})[9].

Probe compounds	$k_{\cdot OH}$	$k_{\cdot SO_4^-}$	$k_{^1O_2}$	Ref.
Benzoic acid (BA)	1.2×10^9	5.9×10^9	-	[9]
Nitrobenzene (NB)	3.9×10^9	$<10^6$	-	[9]
Furfuryl alcohol (FFA)	1.5×10^{10}	1.3×10^{10}	1.2×10^8	[9]
Tetracycline (TC)	4.6×10^9	2.2×10^9	-	[10]

Table S7. The steady-state concentrations and relative ratio of different reactive species to TC degradation in S-Co_3O_4/PMS system.

ROSs	Steady-state concentration (M)	Relative ratio of total ROS (%)
•OH	3.7×10^{-13}	15.6
$\bullet SO_4^-$	1.1×10^{-12}	22.2
$^1O_2$	**6.25×10^{-12}**	**62.2**

1 Y. Zhang, S. T. Zhang, H. A. Li, Y. R. Lin, M. W. Yuan, C. Y. Nan and C. Chen, *Nano Lett.*, 2023, **23**, 9119-9125.

2 T. J. Ni, Z. B. Yang, H. Zhang, L. P. Zhou, W. Guo, D. Liu, K. W. Chang, C. P. Ge and Z. J. Yang, *Appl. Surf. Sci.*, 2022, **604**, 154537.

3 H. Zhang, C. Liu, Y. Wang, F. F. Jia and S. X. Song, *Chem. Phys. Lett*, 2022, **806**, 139996.

4 Z. H. Hu, H. Q. Wu, F. Zhu, S. Komarneni and J. F. Ma, *Inorg. Chem. Commun.*, 2022, **144**, 109902.

5 X. X. Xie, Y. Y. Liu, Y. R. Li, J. Tao, C. Y. Liu, J. P. Feng, L. Feng, Y. X. Shan, S. O. Yang and K. Xu, *J. Taiwan Inst. Chem. Eng.*, 2023, **146**, 104891.

6 P. Xu, S. Q. Xie, X. Liu, L. Wang, R. X. Wu and B. L. Hou, *Chem. Eng. J.*, 2024, **480**, 148233.

7 Y. Q. Wang, K. Li, M. Y. Shang, Y. Z. Zhang, Y. Zhang, B. L. Li, Y. J. Kan, X. Q. Cao and J. Zhang, *Chem. Eng. J.*, 2023, **451**, 138655.

8 B. K. Xu, X. Zhang, Y. Zhang, S. W. Wang, P. Yu, Y. J. Sun, X. Li and Y. H. Xu, *Chem. Eng. J.*, 2023, **466**, 143155.

9 Q. Y. Wu, Z. W. Yang, Z. W. Wang and W. L. Wang, *Proceedings of the National Academy of Sciences of the United States of America*, 2023, **120**, e2219923120.

10 Y. J. Wang, S. Y. Bao, X. Y. Liu, L. Y. Qiu, J. Sheng, W. W. Yang and Y. S. Yu, *Chem. Eng. J.*, 2023, **477**, 147050.